

Quantum Mpemba effect of localization in the dissipative mosaic model

J. W. Dong, H. F. Mu, M. Qin, and H. T. Cui*

School of Physics and Optoelectronic Engineering and Institute of Theoretical Physics, Ludong University, Yantai 264025, China

(Dated: February 19, 2025)

The quantum Mpemba effect in open quantum systems has been extensively studied, but a comprehensive understanding of this phenomenon remains elusive. In this paper, we conduct an analytical investigation of the dissipative dynamics of single excitations in the The mosaic model. Surprisingly, we discover that the presence of an asymptotic mobility edge, denoted as E_c^∞ , can lead to unique dissipation behavior, serving as a hallmark of the quantum Mpemba effect. Especially, it is found that the energy level E_c^∞ exhibits a global periodicity in the real configuration, which acts to inhibit dissipation in the system. Conversely, when the system deviates from E_c^∞ , the quasidisorder sets in, leading to increased dissipative effects due to the broken of periodicity. Furthermore, we find that the rate of dissipation is closely linked to the localization of the initial state. As a result, the quantum Mpemba effect can be observed clearly by a measure of localization.

I. INTRODUCTION

The Mpemba effect (ME) has had a long history of research since its first experimental discovery in 1963[1]. In classical systems, the ME shows that a thermal system at a high temperature T_h can be cooled down to equilibrium faster than one at a low temperature $T_l (< T_h)$ under identical condition. In the quantum realm, the quantum Mpemba effect (QME) characterizes the feature that a quantum system far from equilibrium can relax to equilibrium faster than a system closer to equilibrium. Different methods are used to study the QME, depending on the properties of the system of interest. In closed integrable systems, entanglement asymmetry is used to measure the restoration of symmetry in initially symmetry-broken states [2–9]. The QME can also be observed in quantum simulations, in which systems starting with higher energy can relax faster than those starting with low energy[10].

Another intriguing situation arises in open quantum systems, in which the dissipation can exhibit significant dependence on the initial condition [11–20]. For instance, it was recently found that the approach to the stationary state in Markovian open quantum systems can be exponentially accelerated by performing a unitary transformation [12, 13]. This phenomenon is known as the strong ME, which has been verified experimentally [14]. Furthermore, the QME can also be observed in open nonequilibrium quantum systems, where the system can relax to nonequilibrium steady states (NESS). By measuring the distance to NESS, the QME can be identified by the intersection point of evolution paths at a finite time for distinct initial states [16, 17]. Another interesting the QME was introduced recently, that involves memory time scales induced by the non-Markovian dynamics of an open quantum system [15]. Despite of the observation of the QME in various systems, a general understanding of it remains elusive.

In this paper, we introduce a QME related to the localization in the The mosaic model coupled to a bosonic environment. The mosaic model describes the one-dimensional quasiperiodic lattice system with the sinusoidal disorder appearing on the sites mediated by a unit cell composed of κ sublattices. The mobility edge can be emergent due to the competition between the disorder and periodicity of unit cell. Crucially, the asymptotic mobility edge can be identified, independent of the strength of disorder. As shown in the following discussion, the dissipation of a single excitation can demonstrate the significant correlation to the localization in an initial state due to the presence of asymptotic mobility edge. In contrast to the previous studies, the dissipative dynamics of excitation can be evaluated analytically in this case using Laplace transformation. The exact determination of the effective modes dominating the dynamics provides clear evidence of the QME of localization.

II. MODEL AND METHOD

The mosaic model coupled to a bosonic environment is depicted by the total Hamiltonian

$$H = H_s + H_b + H_{int}. \quad (1)$$

H_s depicts the mosaic model [21], written as

$$H_s = \sum_{n=1}^N \lambda \left(c_n^\dagger c_{n+1} + c_{n+1}^\dagger c_n \right) + \Delta_n c_n^\dagger c_n, \quad (2)$$
$$\Delta_n = \begin{cases} \Delta \cos(2\pi\beta n + \phi), & \text{if } n = j\kappa (j = 1, 2, \dots) \\ 0, & \text{otherwise.} \end{cases}$$

where N denotes the number of lattice and $c_n (c_n^\dagger)$ is the annihilation (creation) operator of the excitation at the n th site. λ characterizes the hopping strength, which is assumed to be unitary in the following. $\beta = (\sqrt{5} - 1)/2$ is the golden ratio, which is responsible for the quasiperiodicity in the system. κ is a positive integer, which denotes the size of the unit cell. When $\kappa = 1$, the mosaic model is reduced to the Abury-André-Harper model

* cuiht01335@aliyun.com

[22, 23], for which the duality symmetry leads to the occurrence of localization-delocalization transition [22, 23]. However, for $\kappa \neq 1$, this symmetry is broken. Thus, the mobility edge (ME) E_c can be determined exactly by [21]

$$|\frac{\Delta}{2}a_k| = 1, \\ a_k = \frac{1}{\sqrt{E_c^2 - 4}} \left[\left(\frac{E_c + \sqrt{E_c^2 - 4}}{2} \right)^\kappa - \left(\frac{E_c - \sqrt{E_c^2 - 4}}{2} \right)^\kappa \right] \quad (3)$$

which separates the extended energy levels from localized ones. In Appendix I, the localization of the mosaic model is depicted in Fig. A1 by the inverse participation ratio. It is observed that as $\Delta \rightarrow \infty$, E_c converges to an asymptotic value E_c^∞ , determined by solving $a_k = 0$. For instance, when $\kappa = 2$, we find that $E_c = \pm \frac{2}{\Delta}$ and $E_c^\infty = 0$, while for $\kappa = 3$, we have $E_c = \pm \sqrt{1 \pm 2/\Delta}$ and $E_c^\infty = \pm 1$. We will show in following that the energy level corresponding to E_c^∞ can exhibit significant resilience to dissipation. Furthermore, the stability of E_c^∞ arises from the inherent discrete translational invariance of the mosaic model. To avoid the boundary effect, the periodic boundary condition $c_{N+n}^{(\dagger)} = c_n^{(\dagger)}$ is imposed in the discussion.

H_b depicts the environment, written as

$$H_b = \sum_k \omega_k b_k^\dagger b_k, \quad (4)$$

where b_k (b_k^\dagger) is the bosonic annihilation (creation) operator for mode k . The coupling between the mosaic model and its environment is depicted by

$$H_{int} = \sum_{k,n} \left(g_k b_k c_n^\dagger + g_k^* b_k^\dagger c_n \right) \quad (5)$$

where g_k are the coupling constants. The open dynamics of the mosaic model is determined by the spectral density

$$J(\omega) = \sum_k |g_k|^2 \delta(\omega - \omega_k). \quad (6)$$

For specification, we choose the Lorentzian spectral density [24] in the following calculation, which has the form

$$J(\omega) = \frac{\eta \omega_c^2}{\omega^2 + \omega_c^2}, \quad (7)$$

where ω_c is the spectrum width and η is the coupling strength. ω is confined to the interval $(-\infty, +\infty)$, allowing for an unbounded spectrum in the environment. This choice rules out the occurrence of discrete bound state [25, 26], which keeps excitation from dissipating by opening an energy gap between the bound state and the spectrum in environment. In this circumstances, the excitation may ultimately be absorbed by the environment, leading to a unique equilibrium in this scenario.

Because of the absence of particle interaction in the mosaic model, the study focuses on the dynamics for a single excitation at zero temperature. In this scenario,

the state of the system and environment can be written in the compact form

$$|\psi(t)\rangle = \left(\sum_{n=1}^N \alpha_n(t) c_n^\dagger + \sum_{k=1}^K \beta_k(t) b_k^\dagger \right) |0\rangle, \quad (8)$$

where $|0\rangle$ is the vacuum state, and K denotes the number of frequency modes in the environment. Substituting Eq. (8) into the Schrödinger equation and solving first for $\beta_k(t)$, one can find an integrodifferential equation for $\alpha_n(t)$,

$$i \frac{\partial}{\partial t} \alpha_n(t) = [\alpha_{n+1}(t) + \alpha_{n-1}(t)] + \Delta_n \alpha_n(t) \\ - i \sum_{n=1}^N \int_0^t d\tau \alpha_n(\tau) f(t - \tau), \quad (9)$$

where $i = \sqrt{-1}$ and

$$f(t - \tau) = \int_0^\infty d\omega J(\omega) e^{-i\omega(t-\tau)}. \quad (10)$$

is the memory kernel.

This equation can be solved both numerically and analytically. The exact numerical evaluation involves discretizing the evolution time equally and finding $\alpha_n(t)$ through iteration. However, this method becomes very exhaustive for long evolution times. Alternatively, Laplace transformation is adopted to find the analytical expression of $\alpha_n(t)$, showing its asymptotic properties. By Laplace transformation

$$A_n(p) = \int_0^\infty dt e^{-pt} \alpha_n(t), \quad (11)$$

Eq. (9) can be rewritten as

$$i [p A_n(p) - \alpha_n(0)] = A_{n+1}(p) + A_n(p) + \Delta_n A_n(p) \\ - i \int_{-\infty}^{+\infty} d\omega \frac{J(\omega)}{p + i\omega} \sum_m A_m(p) \quad (12)$$

which constitutes a linear system of equations for $A_n(p)$ and thus can be solved using Cramer's rule. However, it is noted that the integral $\int_{-\infty}^{+\infty} d\omega \frac{J(\omega)}{p + i\omega}$ becomes divergent when $i p = \omega$. This problem can be resolved by virtue of the Sokhotski-Plemelj (SP) formula

$$\lim_{\epsilon \rightarrow 0} \frac{1}{x - x_0 - i\epsilon} = \text{P} \frac{1}{x - x_0} + i\pi \delta(x - x_0), \quad (13)$$

where P denotes the principle value. One thus gets

$$\lim_{\epsilon \rightarrow 0} \int_{-\infty}^{+\infty} d\omega \frac{J(\omega)}{\omega - ip - i\epsilon} = \text{P} \int_{-\infty}^{+\infty} d\omega \frac{J(\omega)}{\omega - ip} + i\pi J(ip).$$

For instance, one gets, like for the Lorentzian spectral density (7)

$$\int_{-\infty}^{+\infty} d\omega \frac{J(\omega)}{\omega - z} = \frac{\eta \pi \omega_c}{i \omega_c + z},$$

z_i	$\kappa = 2$	$\kappa = 3$
z_1	3.37164 - i 0.193387	3.125206 - i 0.243343
z_2	2.17811 - i 0.0654878	1.896475 - i 0.036575
z_3	1.77457 - i 0.00509817	1.477545 - i 0.002295
z_4	1.22702 - i 0.0119018	<u>1.0 - i 5.07 $\times 10^{-17}$</u>
z_5	0.594323 - i 0.00182872	0.774981 - i 0.004798
z_6	<u>1.06 $\times 10^{-16}$ - i 7.30 $\times 10^{-17}$</u>	-0.126563 - i 0.006496
z_7	-0.0912537 - i 0.00428128	-0.371380 - i 0.00004543
z_8	-0.963238 - i 0.00926696	<u>-1.0 - i 7.16 $\times 10^{-17}$</u>
z_9	-1.13057 - i 0.0016377	-1.13493 - i 0.67839
z_{10}	-1.13266 - i 0.608806	-1.227166 - i 0.0035706
z_{11}	-1.69034 - i 0.0030446	-1.930205 - i 0.00685497
z_{12}	-2.61258 - i 0.00225544	-2.573718 - i 0.0170292
z_{13}	-2.84288 - i 0.00960152	-2.787129 - i 0.000595899

Table I. The poles z solved by finding the zeros of the determinant of the coefficient matrix in Eq. (12). The steady poles are highlighted by underline. For this evaluation, $N = 12$, $\Delta = 2$, $\phi = 0$, $\eta = 0.1$, and $\omega_c = 1$ are chosen.

where $ip = z$ is assumed for convenience.

To determine $\alpha_n(t)$, the inverse Laplace transformation, defined as

$$\alpha_n(t) = \frac{1}{2\pi i} \int_{s-i\infty}^{s+i\infty} dp A_n(p) e^{pt} \quad (14)$$

is applied. Obviously, ip characterizes the effective mode, which determines the single-excitation dynamics. Equation (14) can be evaluated using the residue theorem. For this purpose, one has to find the poles of $A_n(p)$, denoted as $ip_i = z_i$, which are the zero points of the determinant of the coefficient matrix of Eq. (12). Formally, one can get finally

$$\alpha_n(t) \approx \sum_i c_{n,i} e^{-iz_i t}, \quad (15)$$

where $c_{n,i}$ corresponds to the residue of $A_n(p)$ at z_i . It is obvious that the set of poles z_i consists of the dynamical modes, which determines the dissipation of excitation. Especially, the imaginary part of z_i gives rise to the decay rate of excitation, which is responsible for the QME observed in the recent works [12–14]. We emphasize that the summation $\sum_n \alpha_n^*(0) c_{n,i}$ cannot be considered to be the probability on the mode z_i for the initial condition $\{\alpha_n(0)\}$ since the amount of z_i 's is always larger than the dimension of the Hilbert space in the system. Furthermore, it is found that $\sum_n \alpha_n^*(0) c_{n,i}$ can be complex, and moreover the modulus may be larger than unit.

III. DYNAMICAL MODE AND LOCALIZATION IN THE MOSAIC MODEL

With these preparations, we are ready to investigate the single-excitation dynamics in the mosaic model. By

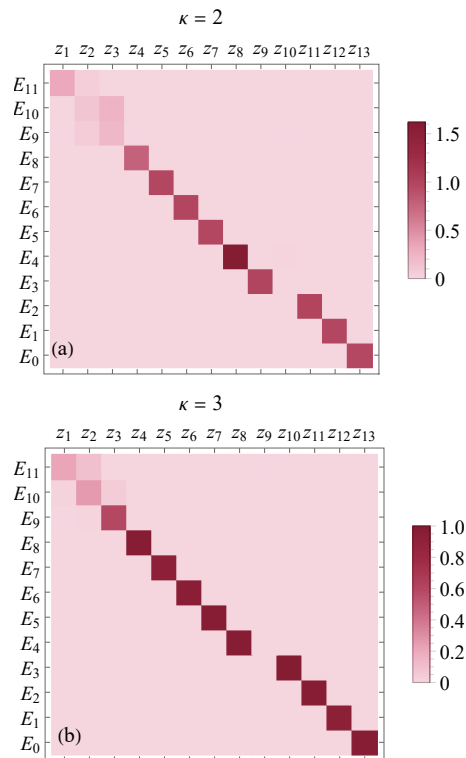


Figure 1. (Color online) The square modulus for the overlap between the energy level E_j ($j = 0, 1, 2, \dots, 11$) (labeled in descending order) in the mosaic model and the coefficient set $\{c_{n,i}\}$ ($n = 1, 2, \dots, N$) related to the initial state $|E_j\rangle$. For the plots, the parameters are chosen to be the same as those in Table I.

setting the determinant of the coefficient matrix to zero, one can derive an equation of degree $N + 1$ for pole z . As an illustration, the solved poles are demonstrated for the case of $\kappa = 2$ and $\kappa = 3$ respectively in Table I with $\Delta = 2$ and $N = 12$. For $\kappa = 2$, one has $E_c = \pm 1$ and for $\kappa = 3$, $E_c = 0, \pm\sqrt{2}$. It is worth noting that all the poles have negative imaginary parts, indicating the dissipative nature of the excitation in the system. An interesting observation is that the imaginary part of the pole is closely related to its corresponding real part. For instance, in the case of $\kappa = 2$, the pole z_6 has a vanishing imaginary part, suggesting that this dynamics mode is resistant to dissipation. Interestingly, its real part tends towards zero, coinciding with the value of E_c^∞ for $\kappa = 2$. It should be emphasized that this coincidence is not occasional, as a similar pattern can be seen for poles z_4 and z_8 for $\kappa = 3$, where their real parts match the value of E_c^∞ for $\kappa = 3$. Apart from the steady poles, the imaginary part of the other poles show a significant increase, indicating varying speeds of dissipation depending on the distance from the steady pole. This suggests that excitations may exhibit different rates of dissipation based on their proximity to the steady pole. Consequently, the QME can be readily observed under these conditions.

It is a natural assumption that the measure of "dis-

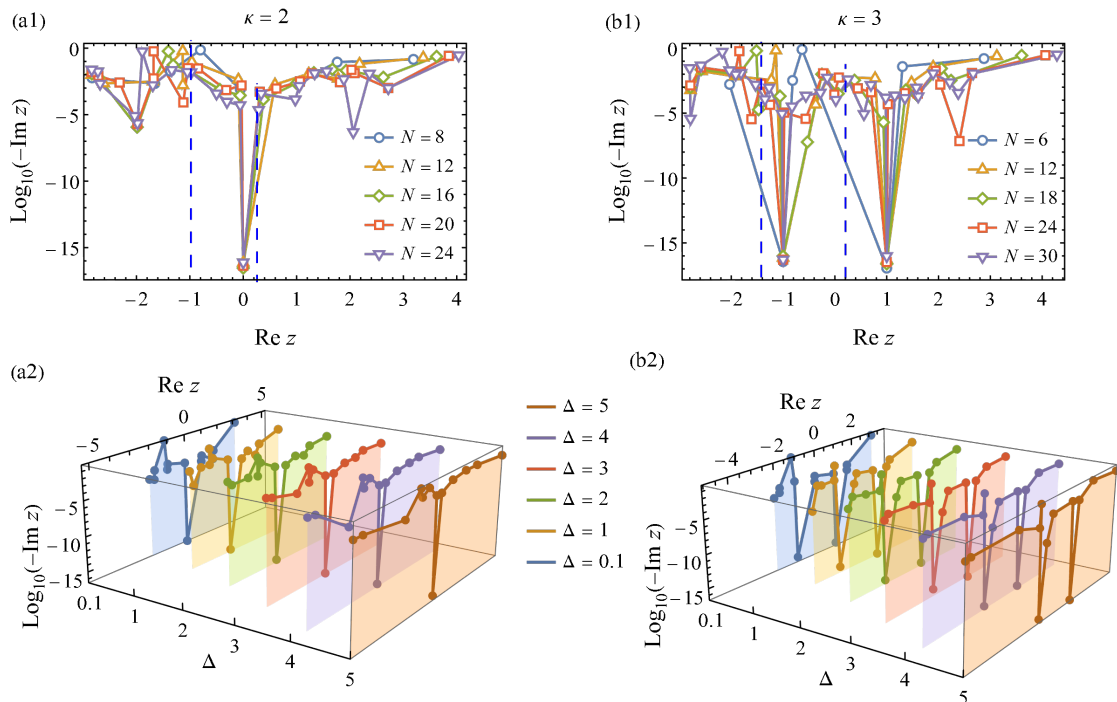


Figure 2. (Color online) The plots for the poles z_i with different Δ 's and N 's. In panels (a1) and (b1), $\Delta = 2$ is chosen. The blue-dashed lines labels the position of $\text{Re } z = E_c$. In panels (a2) and (b2), $N = 12$ is chosen. The other parameters are the same as those in Table I.

tance" is related to the localization in the mosaic model. To confirm this point, the overlap between the energy level E_j ($j = 0, 1, 2, \dots, N - 1$) of the mosaic model and the corresponding coefficient set $\{c_{n,i}\}$ ($n = 1, 2, \dots, N$) for mode z_i , is shown in Fig. 1. According to Eq. (15), this overlap actually characterizes the contribution of mode z_i to the survival probability of the energy eigenstate in the mosaic model for the initial state. As depicted in Fig. 1, the energy level E_j can display a significant overlap with the set $\{c_{n,i}\}$ for a special mode z_i . While the overlap cannot be interpreted as the probability of the initial state on the mode z_i , it does indicate the influence of the dynamic mode z_i on the dissipative evolution of the energy level. This suggests that a particular mode z_i will play a dominant role in the dissipation for a given level E_j for the initial state. In this context, mode z_i may be seen as the renormalization of E_j . Since the level E_j exhibits distinct localizations due to the presence of a mobility edge [21], the dissipation characterized by mode z_i may be seen to be a consequence of localization in the energy level. Therefore, one could adopt the localization as a measure of the deviation of the initial state from equilibrium. The dissipation leads to the system reaching equilibrium by releasing excitation into the environment, ultimately causing the measure of localization to diminish..

Some comments should be made now. First as depicted in Fig. 2, the presence of steady poles z_6 or $z_{4(8)}$ is not influenced by the value of N and Δ , indicating that it

is an inherent characteristic of the mosaic model. To understand the physical basis for the steady poles, we have explicitly calculated the energy levels E_6 for $\kappa = 2$ and $E_{4(8)}$ for $\kappa = 3$ because of their close correspondence to the steady poles, as illustrated in Fig. 1. It is found that the eigenstates corresponding to E_6 and $E_{4(8)}$ exhibit a distinct periodicity in the real configuration, which can be expressed as

$$\begin{aligned}
 |E_6\rangle &= \frac{1}{\sqrt{6}} \left(c_1^\dagger - c_3^\dagger + c_5^\dagger - c_7^\dagger + c_9^\dagger - c_{11}^\dagger \right) |0\rangle \\
 |E_4\rangle &= \frac{1}{2\sqrt{2}} \left(c_1^\dagger + c_2^\dagger - c_4^\dagger - c_5^\dagger + c_7^\dagger + c_8^\dagger - c_{10}^\dagger - c_{11}^\dagger \right) |0\rangle \\
 |E_8\rangle &= \frac{1}{2\sqrt{2}} \left(c_1^\dagger - c_2^\dagger + c_4^\dagger - c_5^\dagger + c_7^\dagger - c_8^\dagger + c_{10}^\dagger - c_{11}^\dagger \right) |0\rangle.
 \end{aligned}$$

In $|E_6\rangle$, only the odd lattice sites can be occupied with a constant phase shift π . This results in a periodic variance by two lattice sites, known as 2-period. On the other hand, both E_4 and E_8 displays the periodic occupation in groups of three consecutive lattice sites, known as 3-period. The periodicity observed in these states is due to the periodic distribution of lattice sites with zero on-site potential, as described by Δ_n in Eq. (2). This periodicity, along with the presence of quasidisorder, leads to the formation of a mobility edge. Thus, it is not surprising that the periodic eigenstate is able to withstand the influence of quasidisorder and remain stable even as the disorder strength approaches infinity, resulting in the

mobility edge E_c^∞ . The stability of these periodic states is protected by the periodicity inherent in the mosaic model. When this periodicity is disrupted, localization occurs, making the poles unstable against dissipation.

Second, there is always an additional pole, such as z_{10} for $\kappa = 2$ and z_9 for $\kappa = 3$ in Table I, where the imaginary part is larger compared to the others. As demonstrated in Fig. 1, this special mode has a minimal impact on the survival probability of energy level E_j of the initial state. In this case, this mode will serve to characterize the scenario of excitation embedded in the environment, thus not affecting the dissipation of excitation in the system. Similarly, the pole with the largest real part also has a finite imaginary part. This mode can be considered to be roughly the renormalized highest excited state in the mosaic model, which decays much faster than the other energy levels.

Finally, in Fig. 2 we observe that the imaginary parts of poles, excluding the additional poles, exhibit a regular variance with respect to the mobility edge E_c . For instance, focusing on the region $|\text{Re}z_i| \leq 1$ in the case of $\kappa = 2$, the poles in this region generally have smaller imaginary parts globally compared to the other poles, as shown in Figs. 2 (a1). However, we also note that the poles near $\text{Re}z_i = \pm 2$ can show the much smaller imaginary parts for a special N . Upon further calculation, it is found that their real parts are very closed to the eigenenergy of The mosaic model in this scenario. Thus, the phenomenon may be attributed to occasional resonance between the dynamical mode and the energy level of the mosaic model, and thus is nonuniversal. A similar trend can be observed in the case of $\kappa = 3$, as shown in Figs. 2 (b1).

IV. QUANTUM MPEMBA EFFECT OF LOCALIZATION

The significant correlation between the dynamical mode and the localization in the mosaic model can give rise to unique dynamics of excitation. To measure the localization of the wave function in the system, the inverse participation ratio (IPR) is introduced, defined as

$$I_\alpha = \sum_n |\alpha_n|^4, \quad (16)$$

where α_n denotes the distribution amplitude of the excitation in the n -th site in the system. IPR reaches its minimum $1/N$ when $|\alpha_n|^2 = 1/N$ for all n , demonstrating a completely extended state. Conversely, the IPR reaches its maximum value of 1 when the excitation is localized on a specific site, indicating complete localization. The time evolution of the IPR is plotted in Fig. 3 for initial states that are chosen to be the energy levels in the mosaic model. From the information in Table I and Fig. 1, it is evident that certain energy levels exhibit significant overlap with special poles, influencing the dissipative dynamics. As shown in Fig. 3, IPR shows varying rates of

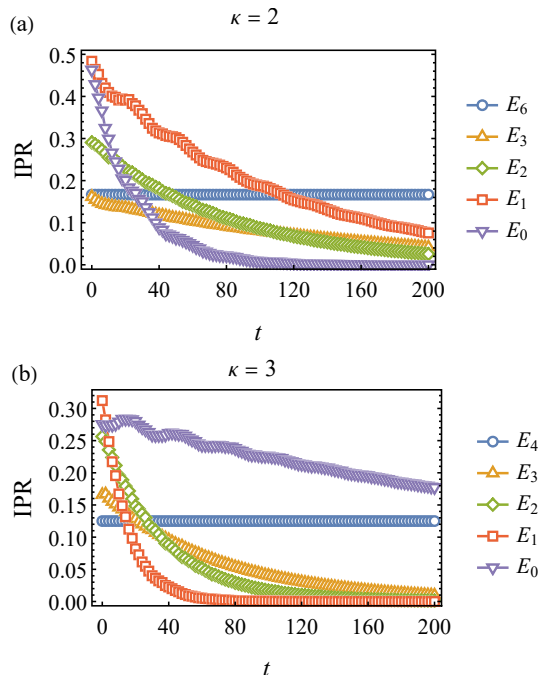


Figure 3. (Color online) The time evolution of IPR for four initial states chosen to be the energy levels in the mosaic model in the cases of $\kappa = 2$ and $\kappa = 3$. The parameters are chosen to be the same as those in Table I.

dissipation for different initial states, determined by the imaginary parts of the corresponding poles. As a result, the evolution paths intersect at certain times, indicating the occurrence of QME [12–14].

It is important to note that the system can be steady in two different scenarios due to the existence of steady poles. In one scenario, when excitation is absorbed by the environment, the system is in equilibrium and IPR tends to be zero, as shown in Figs. 3 (a) and (b) for E_0, E_1, E_2, E_3 . In the other scenario, when the system reaches a steady state, the excitation can remain in the system with a finite probability, and thus IPR can be a finite constant. As shown in Fig. 3 (a) for E_6 and (b) for E_4 , IPR remains constant as the energy levels coincide with the steady pole z_6 for $\kappa = 2$ and z_8 for $\kappa = 3$ respectively. It is worth noting that the QME can be defined only if the initial state with distinct localization decays to the same equilibrium. The presence of steady poles indicates enhanced dissipation due to localization.

Finally, we emphasized that the observed Mpemba effect of localization is purely quantum. The reason can be illustrated by two facets. First, it is well known that the localization of the wavefunction in disordered quantum systems can be attributed to the destructive interference in the quantum amplitudes associated with tunneling paths. Thus, the nonequilibrium in the mosaic model is completely quantum. Second, since the environment is at zero temperature, the decay of the excitation derived from Eq. (9) or (12) is a result of the coherent exchange-

ing of energy between the system and its environment. Especially, the steady mode can emerge from the inherent periodicity in The mosaic model, which is protected by the quasisdisorder. Deviation from the steady mode can lead to the localization of wave function, enhancing the decay of the excitation. In short, the Mpemba effect of localization stems from the interplay of disorder and dissipation and thus is purely quantum.

V. EXPERIMENTAL PROPOSITION

The experimental realization of quasiperiodic the mosaic model was proposed recently in Ref. [27]. In this work, the mosaic lattice can be realized by evanescently coupled waveguides, fabricated on integrated Si₃N₄ photonics platform. The transport properties can be studied by measuring the real-space distribution of light intensity after certain distance of light propagation. The influence of environment can manifest as optical transmission losses, which result from scattering, absorption or dispersion during light propagation. In theory, the losses can be quantified by a propagation coefficient α , which represents the exponential decay of the optical power over distance. This process is physically similar to the spontaneous emission of atomic excitation, which can be captured by a virtual environment with the Lorentz spectral function. By determining the value α , one can identify the influence of the energy mode z . As for the steady mode, α may vanish or be negligible, while a finite α can occur for the other modes.

In light of the experiment, special focus should be placed on preparing steady modes like $|E_6\rangle$, $|E_4\rangle$, and $|E_8\rangle$ in Sec.III. It is clear that achieving strict periodicity and consistent phase shifts in the steady mode necessitates meticulous preparation of the waveguide structure. Additionally, it is important to note that the quasiperiodic the mosaic model is subject to the periodic boundary condition $c_{N+n}^{(\dagger)} = c_n^{(\dagger)}$, which may pose inconveniences in experimental settings.

VI. CONCLUSION AND DISCUSSION

In conclusion, the single-excitation dynamics in the mosaic model coupled to a bosonic environment was studied analytically in this paper by determining the dynamical modes. We found that the dynamical modes are closely tied to the energy levels in the mosaic model. Furthermore, due to the existence of robust asymptotic mobility edge, the dynamics of the excitation displays a significant correlation to the localization in the mosaic model. Especially, we observe that the asymptotic mobility edge E_c^∞ corresponds to a steady dynamical mode, which shows vanishing imaginary part, meaning it is dissipationless. The energy level E_c^∞ also exhibits a global periodicity in real configuration, determined by the spatial period in the mosaic model. Apart from E_c^∞ , the

dynamical mode shows finite imaginary part, reflecting the dissipative dynamics. This suggests a relationship between the dissipative dynamics of excitation and the localization properties of the mosaic model. By adopting the IPR as a measure of localization, the paths of evolution for the IPR can intersect at different times for various initial states, highlighting the localization-related QME.

Although this study centered on the single-excitation case, the dynamics for multiple excitations does not exhibit essential differences as a result of the absence of particle interaction. This can be confirmed by observing that the state of multiple excitations can always be expressed as a product form of single excitation states when there is no particle interaction. For convenience, the single excitation is rewritten as

$$|1_n\rangle = \left(\sum_{j=1}^N \alpha_{n,j} c_n^\dagger + \sum_{k=1}^K \beta_{n,k} b_k^\dagger \right) |0\rangle := \hat{e}_n |0\rangle, \quad (17)$$

satisfying $H|1_n\rangle = E_n^{(1)}|1_n\rangle$. With this formula, the total Hamiltonian can be expressed as

$$H = \sum_n E_n^{(1)} \hat{e}_n^\dagger \hat{e}_n. \quad (18)$$

As an example, the energy state for double excitations can be written explicitly as

$$|2_n\rangle = \hat{e}_i \hat{e}_j |0\rangle. \quad (19)$$

It is not difficult to get

$$H|2_n\rangle = \left(E_i^{(1)} + E_j^{(1)} \right) |2_n\rangle. \quad (20)$$

This observation suggests that the effective mode for double excitations could be a combination of two single excitation modes, leading to an increased decay rate as a sum of the single excitation rates. A state of multiple excitations can be formed in a similar manner.

It should be pointed out that mobility edge can emerge through the introduction of short-term [28] or long-term hopping [29], or the breaking the duality symmetry [30–33] in the Aubry-André-Haper model [22, 23]. Different from the The mosaic model, the mobility edges in these cases generally show dependence on the quasisdisordered on-site potential, and there is no asymptotic mobility edge. Since the occurrence of dissipation is independent of the potential, it is impossible to establish the relationship between the localization and the decay. Our investigation of the single excitation dynamics in the generalized Aubry-André-Haper model introduced in Ref. [31] confirms this hypothesis, as shown in Appendix II.

Finally, it is crucial for the QME of the localization that the extended energy level E_c^∞ can withstand dissipation and exhibit the periodicity related to the value of κ in the the mosaic model. In physics, the robustness of the energy level E_c^∞ is a result of the homogeneous coupling

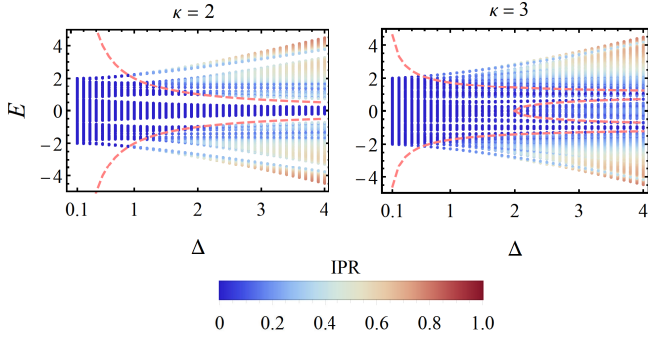


Figure A1. (Color online) The plot of IPR for all energy levels in the the mosaic model in the cases of $\kappa = 2$ and $\kappa = 3$ respectively. The dashed-pink line characterizes the mobility edge, determined by Eq. (3). For the plots, $N = 610$, $\Delta = 2$ and $\phi = 0$ are chosen.

of the lattice to the environment, as shown in Eq.(5), keeping the global periodicity in the mosaic model invariant. This suggests that the asymptotic mobility edge may persist beyond the single-excitation subspace or in the presence of particle interaction. However, exploring multiple-excitation dissipative dynamics in interacting many-body systems poses a theoretical challenge that remains to be addressed by future research.

ACKNOWLEDGEMENTS

H.T.C. acknowledges the support of the Natural Science Foundation of Shandong Province under Grant No. ZR2021MA036. M.Q. acknowledges the support of NSFC under Grant No. 11805092 and the Natural Science Foundation of Shandong Province under Grant No. ZR2018PA012.

Appendix I. THE LOCALIZATION OF ENERGY LEVEL IN THE THE MOSAIC MODEL

In this appendix, a brief discussion of the localization in the the mosaic model is presented. It is known that due to the existence of mobility edge, the energy levels in the the mosaic model can exhibit unique localization characteristics. We adopt the inverse participation ratio defined by Eq. (16) to quantify the localization in the system. As shown in Fig. A1, the energy level of the system can exhibit either localized or extended behavior depending on its position relative to the mobility edge. The coexistence of localized and extended state is a typical feature for the the mosaic model, leading to the complex dynamics in the system.

The presence of E_c^∞ in the the mosaic model is a result of the periodicity, decided by the onsite potential Δ_n in Eq. (2). It has been observed that E_c^∞ is one of the eigenvalues of H_s only when N/κ is even. In physics, the

z_i	$a = 0.5$	$a = -0.5$
z_1	4.46302 - i 0.04866	2.79814 - i 0.21174
z_2	3.22087 - i 0.06612	1.72400 - i 9.101 $\times 10^{-5}$
z_3	2.27772 - i 0.02594	1.70546 - i 1.913 $\times 10^{-4}$
z_4	0.41668 - i 0.05686	-0.11475 - i 0.006911
z_5	0.28352 - i 0.05176	-0.27667 - i 0.03026
z_6	-0.57714 - i 0.67695	-0.68474 - i 0.72597
z_7	-1.70351 - i 6.235 $\times 10^{-5}$	-2.45659 - i 0.00369
z_8	-1.85742 - i 0.073562	-3.47499 - i 0.01309
z_9	-2.0735 - i 8.954 $\times 10^{-5}$	-4.00698 - i 0.00802

Table AI. The effective mode z for GAAH defined by Eq. (A1). For this evaluation, $N = 8$, $\Delta = 2$, $\phi = \pi$, $\eta = 0.1$, and $\omega_c = 1$ are chosen.

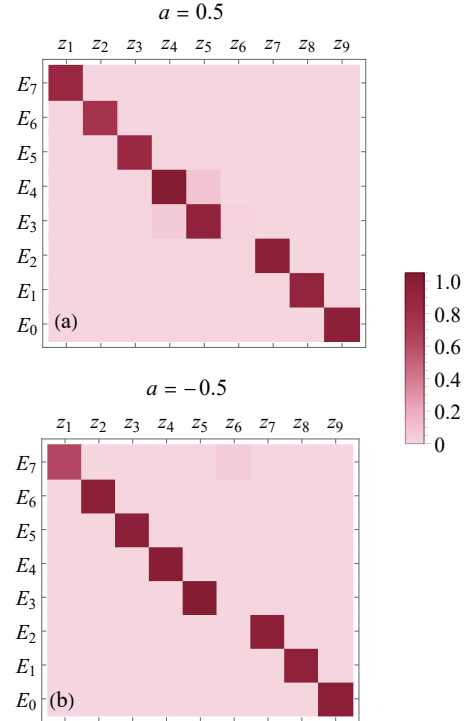


Figure A2. (Color online) The square modulus for the overlap between the energy level E_j ($j = 0, 1, 2, \dots, 7$ in descending order) in the GAAH model and the coefficient set $\{c_{n,i}\}$ ($n = 1, 2, \dots, 8$) related to the initial state $|E_j\rangle$, defined by Eq.(15). For the plots, the parameters are chosen the same as those in Table I. For $a = 0.5$, $E_j > 0$ when $j = 3, 4, 5, 6, 7$, while $E_j < 0$ otherwise. In contrast, for $a = -0.5$, $E_j > 0$ when $j = 5, 6, 7$, while $E_j < 0$ otherwise.

The mosaic model depicts a lattice system that shows both disorder and invariant by discrete translation. It is obvious from the definition of Δ_n that the disorder presents only at the site $n = j\kappa$, while the discrete translation invariance occurs for the other sites. The interplay between disorder and discrete translation invariance gives rise to the emergence of the mobility edge.

Appendix II. EFFECTIVE MODES IN THE GENERALIZED AUBRY-ANDRÉ-HARPER MODEL

To demonstrate the special role of E_∞ , we evaluate the effective modes in the generalized Aubry-André-Harper (GAAH) model [31], in which the Hamiltonian is

$$H_s = \sum_{n=1}^N c_n^\dagger c_{n+1} + c_{n+1}^\dagger c_n + \frac{\Delta \cos(2\pi\beta n + \phi)}{1 - a \cos(2\pi\beta n + \phi)} c_n^\dagger c_n \quad (\text{A1})$$

where N denotes the number of lattice sites and c_n (c_n^\dagger) is the annihilation (creation) operator of the excitation at the n -th lattice site. The hopping strength is assumed to be unity. The onsite potential is a smooth function of parameter a in the open interval $a \in (-1, 1)$. When $a = 0$, Eq. (A1) reduces to the standard Aubry-André-Harper model. However, the GAAH model exhibits an exact mobility edge when $a \neq 0$, determined by

$$aE_c = \text{sgn}(\lambda) (2|\lambda| - |\Delta|). \quad (\text{A2})$$

Depending on whether $a > 0$ or $a < 0$, the energy levels display much localization with the increasing or decreasing of E_j . By choosing $\Delta = 2$, one gets $E_c = 0$.

As an illustrations, we investigate the effective modes for $a = 0.5$ and $a = -0.5$ respectively by using the method in Section II. Furthermore, we also check the overlap between the coefficient set $\{c_{n,i}\}$ ($n = 1, 2, \dots, N$) for mode z_i and the energy level E_j ($j = 0, 1, 2, \dots, N - 1$, labeled in descending order) in the GAAH model in Fig. A2, which clearly illustrate the

relationship between the effective modes and the energy levels in the GAAH model. Evidently, for both $a = 0.5$ and -0.5 , there is an additional mode z_6 with a very large imaginary part. Because z_6 show negligible overlap with the energy level in the system, it will serve to characterize the scenario of excitation embedding in the environment, thus not affecting the dissipation of the excitation initially in the system.

As for the other modes, there is no evidence for a relationship between the decay rate and localization. For example, z_1 show a significantly larger decay rate than those for z_2 and z_3 , as shown for $a = -0.5$ in Table AI. Additionally, there is a great overlap with the known extended levels $E_j > 0$, shown in Fig. A2(b), indicating that the decay of excitation is irrelevant to the localization of system. Similar observation can be made for z_7, z_8 and z_9 when $a = 0.5$, as shown in the second column in Table AI.

One main difference of the GAAH model from the the mosaic model is the absence of E_c^∞ . In the GAAH model, $E_c \rightarrow \pm\infty$ as $\Delta \rightarrow \infty$ following Eq. (A2), leading to all energy levels becoming localized. This feature implies that the dissipation induced by coupling to the environment will be irrelevant to the property of localization. Thus, the QME of localization cannot occur in the GAAH model. On the other hand, the The mosaic model includes E_c^∞ , ensuring the existence of extended states even as Δ approaches infinity. Importantly, the energy level E_c^∞ is robust against dissipation. This difference allows for a relationship to be established between the decay of excitation and localization by measuring the "distance" from E_c^∞ . Manifestly, the localization can perfectly serve as the measure.

-
- [1] E. B. Mpemba and D. G. Osborne, Cool?, Phys. Educ. **4**, 172 (1969).
- [2] F. Ares, S. Murciano, and P. Calabrese, Entanglement asymmetry as a probe of symmetry breaking, Nat. Commun. **14**, 2036 (2023).
- [3] S. Murciano, F. Ares, I. Klich, and P. Calabrese, Entanglement asymmetry and quantum mpemba effect in the XY spin chain, J. Stat. Mech., 013103 (2024).
- [4] F. Ares, S. Murciano, E. Vernier, and P. Calabrese, Lack of symmetry restoration after a quantum quench: An entanglement asymmetry study, SciPost Phys. **15**, 089 (2023).
- [5] K. Chalas, F. Ares, C. Rylands, and P. Calabrese, Multiple crossing during dynamical symmetry restoration and implications for the quantum mpemba effect, J. Stat. Mech. 103101 (2024).
- [6] C. Rylands, K. Klobas, F. Ares, P. Calabrese, S. Murciano, and B. Bertini, Microscopic origin of the quantum mpemba effect in integrable systems, Phys. Rev. Lett. **133**, 010401 (2024).
- [7] Lata Kh. Joshi, J. Franke, A. Rath, F. Ares, S. Murciano, F. Kranzl, R. Blatt, P. Zoller, B. Vermersch, P. Calabrese, Christian F. Roos, and Manoj K. Joshi, Observing the Quantum Mpemba Effect in Quantum Simulations, Phys. Rev. Lett. **133**, 010402 (2024).
- [8] S. Liu, H.-K. Zhang, S. Yin, S.-X. Zhang, and H. Yao, Quantum Mpemba effects in many-body localization systems, arXiv: 2408.07750 (2024).
- [9] S. Liu, H.-K. Zhang, S. Yin, S.-X. Zhang, Symmetry restoration and quantum Mpemba effect in symmetric random circuits, Phys. Rev. Lett. **133**, 140405 (2024).
- [10] W.-X. Chang, S. Yin, S.-X. Zhang, and Z.-X. Li, Imaginary-time Mpemba effect in quantum many-body system, arXiv: 2409.06547 (2024).
- [11] Z. Lu and O. Raz, Nonequilibrium thermodynamics of the Markovian Mpemba effect and its inverse, Proceedings of the National Academy of Sciences **114**, 5083 (2017).
- [12] F. Carollo, A. Lasanta, and I. Lesanovsky, Exponentially accelerated approach to stationarity in markovian open quantum systems through the mpemba effect, Phys. Rev. Lett. **127**, 060401 (2021).
- [13] S. Kochsiek, F. Carollo, and I. Lesanovsky, Accelerating the approach of dissipative quantum spin system towards stationarity through global spin rotations, Phys. Rev. A **106**, 012207 (2022).

- [14] Jie Zhang, Gang Xia, Chun-Wang Wu, Ting Chen, Qian Zhang, Yi Xie, Wen-Bo Su, Wei Wu, Cheng-Wei Qiu, Ping-Xing Chen, Weibin Li, Hui Jing, and Yan-Li Zhou, Observation of quantum strong Mpemba effect, *Nat. Commun.* **16**, 301 (2025).
- [15] D. J. Strachan, A. Purkayastha, and S. R. Clark, Non-Markovian quantum Mpemba effect, arXiv: 2402.05756 (2024).
- [16] A. Nava, adna R. Egger, Mpemba effect in open nonequilibrium quantum systems, *Phys. Rev. Lett.* **133**, 136302 (2024).
- [17] X. Wang and J. Wang, Mpemba effect in nonequilibrium open quantum system, *Phys. Rev. Research* **6**, 033330 (2024).
- [18] A. K. Chatterjee, S. Takada, and H. Hayakawa, Quantum Mpemba Effect in a Quantum Dot with Reservoirs, *Phys. Rev. Lett.* **131**, 080402 (2023).
- [19] A. K. Chatterjee, S. Takada, and H. Hayakawa, Multiple quantum Mpemba effect: exceptional points and oscillations, *Phys. Rev. A* **110**, 022213 (2024).
- [20] X. Wang, J. Su and J. Wang, Mpemba meets quantum chaos: Anomalous relaxation and Mpemba crossings in dissipative Sachdev-Ye-Kitaev models, arXiv: 2410.06669 (2024).
- [21] Y.-P. Wang, X. Xia, L. Zhang, H.-P. Yao, S. Chen, J.-G. You, Q. Zhang and X.-J. Liu, One-dimensional quasiperiodic The mosaic Lattice with exact mobility edges, *Phys. Rev. Lett.* **125**, 196604 (2020).
- [22] S. Aubry and G. André, Analyticity Breaking and Anderson Localization in Incommensurate Lattices, *Ann. Isr. Phys. Soc.* **3**, 133 (1980);.
- [23] P. G. Haper, Single Band Motion of Conduction Electrons in a Uniform Magnetic Field, *Proc. Phys. Soc. London Sect. A* **68**, 874 (1955)
- [24] B. Bellomo, R. Lo Franco, and G. Compagno, Non-Markovian Effects on the Dynamics of Entanglement, *Phys. Rev. Lett.* **99**, 160502 (2007).
- [25] E. Yablonovitch, Inhibited Spontaneous Emission in Solid-State Physics and Electrics, *Phys. Rev. Lett.* **58**, 2059-2062 (1987).
- [26] S. John and J. Wang, Quantum Electrodynamics near a Photonic Band Gap: Photon Bound States and Dressed Atoms, *Phys. Rev. Lett.* **64**, 2418-2421 (1990).
- [27] J. Gao, I.M. Khaymovich, X.-W. Wang, Z.-S. Xu, A. Iovan, G. Krishna, J. Jieesi, A. Cataldo, A. V. Balatsky, V. Zwiller, and Ali W. Elsharri, Probing multi-mobility edges in quasiperiodic the mosaic lattices, *Science Bulletin*, <https://doi.org/10.1016/j.scib.2024.09.030>.
- [28] J. Biddle and S. Das Sarma, Predicted Mobility Edges in One-dimensional Incommensurate Optical lattices: An Exactly Solvable Model of Anderson Localization, *Phys. Rev. Lett.* **104**, 070601 (2010).
- [29] X. Deng, S. Ray, S. Sinha, G. V. Shlyapnikov, and L. Santos, One-Dimensional Quasicrystals with Power-Law Hopping, *Phys. Rev. Lett.* **123**, 025301 (2019).
- [30] S. Das Sarma, Song He, and X. C. Xie, Mobility Edge in a Model One-Dimensional Potential, *Phys. Rev. Lett.* **61**, 2144 (1988).
- [31] S. Ganeshan, J. H. Pixley, and S. Das Sarma, Nearest Neighbor Tight Binding Models with an Exact Mobility Edge in One Dimension, *Phys. Rev. Lett.* **114**, 146601 (2015).
- [32] X. Li, X.-P Li, and S. Das Sarma, Mobility edges in one-dimensional bichromatic incommensurate potentials, *Phys. Rev. B* **96**, 085119 (2017).
- [33] H. Yao, A. Khoudli, L. Bresque, and L. Sanchez-Palencia, Critical Behavior and Fractality in Shallow One-Dimensional Quasiperiodic Potentials, *Phys. Rev. Lett.* **123**, 070405 (2019).